



Cite this: *RSC Adv.*, 2023, **13**, 26709

Inhibitory selectivity to the AKR1B10 and aldose reductase (AR): insight from molecular dynamics simulations and free energy calculations†

Ping Lin^{*ab} and Yuzhen Niu  ^{*ac}

AKR1B10 is over-expressed in many cancer types and is related to chemotherapy resistance, which makes AKR1B10 a potential anti-cancer target. The high similarity of the protein structure between AKR1B10 and AR makes it difficult to develop highly selective inhibitors against AKR1B10. Understanding the interaction between AKR1B10 and inhibitors is very important for designing selective inhibitors of AKR1B10. In this study, Fidarestat, Zopolrestat, MK184 and MK204 bound to AKR1B10 and AR were used to investigate the selectivity mechanism. The results of MM/PBSA calculations show that van der Waals and electrostatic interaction provide the main contributions of the binding free energy. The hydrogen bonding between residues Y49 and H111 and inhibitors plays a pivotal role in contributing to the high inhibitory activity of AKR1B10 inhibitors. The π - π stacking interaction between residue W112 and inhibitor also plays a key role in the stability of inhibitors and AKR1B10, but W112 should keep its natural conformation to stabilize the inhibitor-AKR1B10 complex. Highly selective AKR1B10 inhibitors should have a bulky moiety like a phenyl group, which can change its binding with ABP in binding with AR and cannot change its binding with AKR1B10. The free energy decomposition shows that residues W21, V48, Y49, K78, W80, H111, R298 and V302 are beneficial to the stability of the inhibitor-AKR1B10. Our work will provide an important *in silico* basis for researchers to develop highly selective inhibitors of AKR1B10.

Received 4th April 2023

Accepted 23rd June 2023

DOI: 10.1039/d3ra02215c

rsc.li/rsc-advances

1. Introduction

AKR1B10 (human aldo-ketoreductase family1, Member 10)¹ and AKR1B1 (human aldo-ketoreductase family1, Member 1, also named aldose reductase, AR)² are two members of the AKR1 subfamily B, and the homology between AKR1B10 and AR is 70.89%.³ The human AR is the key enzyme of the polyol pathway, which catalyzes the reduction of glucose to sorbitol with high glucose concentration.⁴ The overexpression of AR is related to the secondary complications of diabetes,^{5,6} and it is expressed in various tissues of the human body, so AR inhibitors are mainly used to treat the complications related to diabetes at present.⁷ However, the overexpression of AKR1B10 in various human tissues is obviously selective.^{8,9} For example, AKR1B10 is over-expressed in 70% of pancreatic cancer and tumor-like lesions in pancreatic epithelium.¹⁰ AKR1B10 is also over-expressed in erosive epithelium of esophagus and Barrett's

epithelium, and further deterioration of this can lead to the occurrence of esophageal cancer.^{11,12} In addition, AKR1B10 is also expressed in the small intestine and colon,¹³ but at a low level in the liver, prostate, testis and thymus, while it is basically not expressed in most other normal human tissues.¹⁴ Therefore, AKR1B10 has become a potential target of anti-tumor drugs in recent years, and the research of its inhibitors has also brought new opportunities for tumor treatment.¹ Moreover, AKR1B10 inhibitors can also affect the sensitivity of tumor cells to chemotherapeutic drugs, which can find a new way to improve the effect of tumor chemotherapy.¹⁵ Therefore, with the in-depth study of AKR1B10 and its inhibitors, finding efficient and selective AKR1B10 inhibitors will certainly bring new hope for the diagnosis and treatment of tumors.¹⁶⁻¹⁸

Because of the high similarity of amino acid sequences of AKR1B10 and AR, the three-dimensional structure of them is also similar, which means that commonly developed inhibitors can both bind to AKR1B10 and AR. Selectivity is one of the most important factors affecting side effects in drug design,¹⁹ and it is extremely difficult to obtain selectivity in protein which belongs to the same family and has high sequence similarity.²⁰ Therefore, considering the selective expression of AKR1B10 and AR in different tissues, it is necessary to improve the specificity of AKR1B10 inhibitors for anti-cancer by targeting AKR1B10. At present, relevant research on selective inhibitors of AKR1B10 is

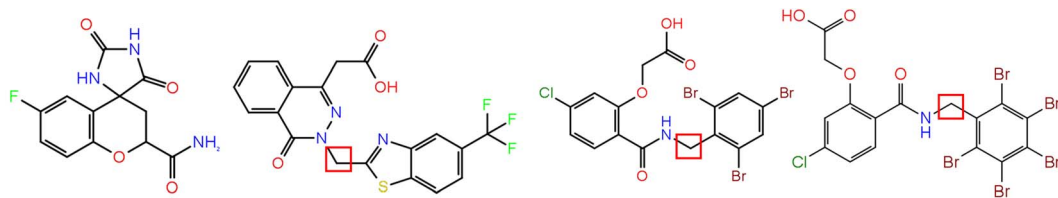
^aWeifang University of Science and Technology, Weifang, 262700, China. E-mail: linping07@mails.ucas.ac.cn; niuyzh12@lzu.edu.cn

^bInstitute of Modern Physics, Chinese Academy of Science, Lanzhou 730000, China

^cShandong Engineering Research Center of Green and High-value Marine Fine Chemical, Weifang University of Science and Technology, Weifang, 262700, China

† Electronic supplementary information (ESI) available. See DOI: <https://doi.org/10.1039/d3ra02215c>





Fidarestat (1)

Zopolrestat (2)

MK184 (3)

MK204 (4)

Inhibitor	IC ₅₀ (μM)		AKR1B10 selectivity
	AKR1B10	AR	
Fidarestat	33 (com1)	0.026 (com2)	0.0008
Zopolrestat	0.62 (com3)	0.018 (com4)	0.029
MK184	1.0 (com5)	21.4 (com6)	21.0
MK204	0.08 (com7)	21.7 (com8)	271.25

Fig. 1 Chemical structures and biological activity to AKR1B10 and AR of inhibitors studied in this work.

still scarce, and the researchers try to use AR inhibitors to inhibit the activity of AKR1B10. Fidarestat (1) and Zopolrestat (2) are AR inhibitors^{21,22} (Fig. 1), which are used to treat diabetic neuropathy clinically. However, the inhibitory activities of these two compounds on AKR1B10 and AR have no obvious difference. MK184 (3) and (4) are two only compounds with high selectivity to AKR1B10 reported to date.^{23,24} The crystal structures of Zopolrestat binding with AKR1B10 and AR, Fidarestat combined with AR and MK184 binding with AKR1B10 have been determined by X-ray crystallography. Although this structural data is necessary to clarify the inhibition mechanism, the data obtained from the crystal structure is limited, because the crystal structure can only provide a single instantaneous conformation of the complex. Therefore, it is necessary to further clarify the interaction in the kinetic complex of protein or protein–inhibitor complex. Molecular dynamics (MD) simulations, which can be used to observe the dynamic behavior of biomolecules, studies not only the stable snapshot interaction, but also includes the dynamic interaction between the residues and inhibitors and to clarify the mechanism of inhibitor selectivity.

Therefore, in this work, we have carried out MD simulations to study the binding of four compounds (Fidarestat, Zopolrestat, MK184 and MK204) to AKR1B10 and AR, and calculated the binding free energy of the equilibrated parts of MD trajectories to clarify the key binding characteristics of compounds with high selectivity to AKR1B10. We got the stable conformation of MK204 binding to AKR1B10 and AR from MD simulations, and strengthened the difference of binding modes between them. We identified the key residues of AKR1B10 and AR contributed to inhibitors binding and estimated the difference of their impact to the binding free energy. Finally, we summarized the binding characteristics of AKR1B10 inhibitors with high selectivity. There is only a few activity test data of AKR1B10 and AR at present, and we believe that our work will provide an important data for researchers to develop highly selective inhibitors of AKR1B10.

2. Materials and methods

2.1 Molecular docking

The crystal structures of Fidarestat/AR, MK184/AR and MK204/AR complexes were not found in PDB database, so we tried to get the initial poses for the four complexes by molecular docking. The molecular docking was performed with Glide in Schrödinger 2015 (Schrödinger, LLC, New York, NY, USA). The crystal structure of Zopolrestat/AR complex (PDB ID: 4JII²⁵) was used to define the docking grid box for AR protein, while the MK184/AKR1B10 was used to define the docking grid box for AKR1B10, and the ligands were docked into the defined docking pocket using Glide with standard precision (SP) and extra precision (XP). The docking pose with the highest score was selected as their initial binding pose for further evaluation.

Induced Fit Docking (IFD)^{26,27} was performed in Schrödinger 2015 to get more accurate initial pose. The protein molecule was minimized with an RMSD cutoff of 0.2 Å, and then was generated the centroid of the residues automatically. The initial docking for each ligand was carried out with Glide. The residues within 5.0 Å of the ligand position are restricted to optimize the side chain. The ligand is strictly docked into the protein structure suitable binding pocket, and as a result, the IFD score of each output posture is generated.

2.2 Molecular dynamics (MD) simulations

2.2.1 Complex setup. The starting structure of the Zopolrestat/AKR1B10, Zopolrestat/AR, Fidarestat/AKR1B10, MK184/AKR1B10 and MK204/AKR1B10 complexes were obtained from the RCSB Protein Data Bank (PDB ID code is 4JII,²⁵ 2DV0,²⁸ 1PWM,²⁹ 5LIX²³ and 5LIY,²³ respectively). The missing residues were added and aligned together using Schrödinger 2015. Then the structure of the complexes was prepared by the Protein Preparation Wizard, including adding side chain of residues, hydrogen atoms, assigning protonation states, and relaxing the amino residue side chains of the proteins. The



starting structure of Fidarestat/AR, MK184/AR and MK204/AR were obtained using the Glide.

The partial charges of the four ligands were computed at the HF/6-31G(d) level of theory and fixed using the RESP methodology.³⁰⁻³² Each receptor-ligand construct was finally parameterized using the AMBER14SB³³ and GAFF force fields. Then, the complexes were solvated with TIP3P water models³⁴ in a 10 Å cubic box using Leap, and Na⁺ ions were added to neutralize the net charge of the complex.

2.2.2 Equilibration and production runs. All of the MD simulations were performed with the Amber20 simulation package. The specific parameter settings refer to our previous work. Particle Mesh Ewald (PME) algorithm³⁵ was employed to treat long-range electrostatic interactions, while the cutoff for the short-range non-bonded interactions were set to 10 Å. All bonds involving hydrogen atoms were restrained using the SHAKE algorithm,³⁶ and the time step was set to 2 fs. 1000 ns MD simulations at a temperature of 310 K and a pressure of 1 atm were carried out without any restrain. During the sampling process, the coordinates of each complex were saved every 10 ps.

2.3 MM/PBSA binding free energy calculations and residue decomposition

The Molecular Mechanics with Poisson–Boltzmann/Surface Area (MM/PBSA) method,^{37,38} widely used in estimating receptor and ligand interaction binding, was employed to estimate the binding free energies for the receptor and ligand interaction.^{39–46} In MM/PBSA method, the binding free energy

can be decomposed into several terms, including the bond, angle, torsion, van der Waals, and electrostatic terms. In MM/PBSA calculations, 2000 snapshots were extracted from the last 200 ns MD trajectory (take one at every 10 snapshots) for the free energy calculations. The binding free energy can be calculated as follows:

$$\langle \Delta G_{\text{bind}} \rangle \langle \Delta E_{\text{bond}} \rangle + \langle \Delta E_{\text{angle}} \rangle + \langle \Delta E_{\text{tors}} \rangle + \langle \Delta E_{\text{vdw}} \rangle + \langle \Delta E_{\text{ele}} \rangle + \langle \Delta G_{\text{PB}} \rangle + \langle \Delta G_{\text{SA}} \rangle - T \langle \Delta S_{\text{MM}} \rangle \quad (1)$$

where $\langle \Delta G_{\text{bind}} \rangle$ is the calculated average free energy, and the polar contribution of solvation ($\langle \Delta G_{\text{PB}} \rangle$) was calculated based on Poisson–Boltzmann (PB) model.⁴⁷ The nonpolar contribution of solvation ($\langle \Delta G_{\text{SA}} \rangle$) was determined by solvent accessible surface area (SASA) using the LCPO method: $\Delta G_{\text{SA}} = 0.0072 \times \Delta \text{SASA}$. The conformational entropy contribution ($-T\langle \Delta S \rangle$) upon ligand binding is calculated using normal-mode analysis⁴⁸ in AMBER20. All steps of minimizations and normal-mode calculation were performed with a distance-dependent dielectric function $4R_{ij}$ (the distance between two atoms) to mimic solvent screening. The structures were further minimized with no cutoff for non-bonded interactions by using conjugate gradient and then Newton–Raphson minimizations until the RMS of the elements in the gradient vector was less than 10^{-4} kcal (mol $^{-1}$ Å $^{-1}$). Due to the high computational cost in the entropy calculation, only 50 snapshots were extracted from the last 200 ns MD trajectory was used to calculate the entropic contribution (take one at every 400 snapshots).

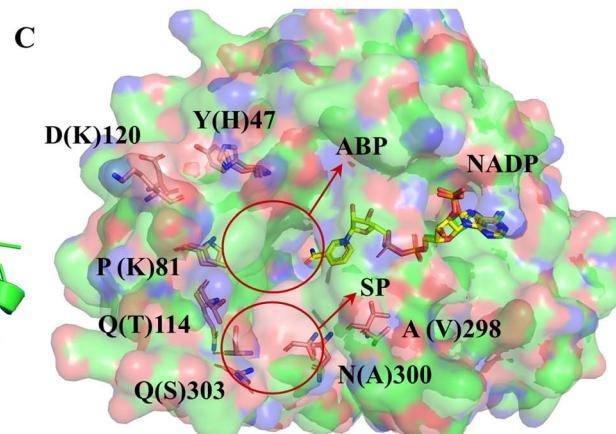
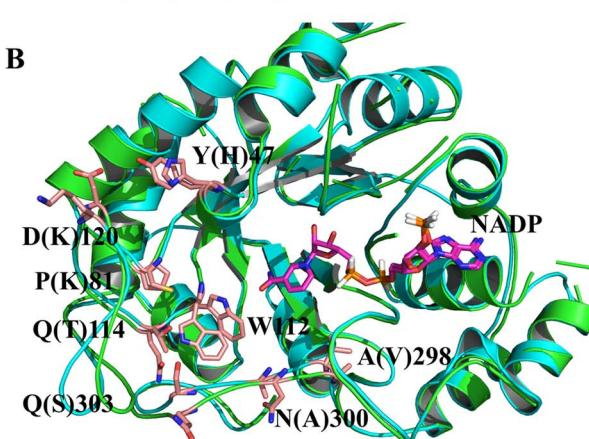


Fig. 2 Comparison of the amino acid sequence (A) and the protein structure between AKR1B10 and AR (B) and (C). ABP: anion binding pocket; SP: specificity pocket.

3. Results and discussion

3.1 Summary the structural characteristics of AKR1B10 and AR

As is shown in Fig. 2, AKR1B10 and AR share an $(\alpha/\beta)8$ -barrel core motif, which are conserved in metabolic enzymes. Residues Y49, K77, H111 and W112 define a geometrically rigid “anion binding pocket (ABP)” with the nicotinamide moiety of NADP⁺, which is the conventional binding site of AKR1 inhibitors. Sequence alignment of AKR1B10 and AR shows 71% amino acid identity, and superposition of the 3D structures of AKR1B10 and AR shows that the differences mainly come from the three-segment loop regions, including loop A (residues 110–138), loop B (residues 210–232) and loop C (residues 292–316). The three external and highly variable loops contribute to protein plasticity, substrate specificity and inhibitor selectivity. Meanwhile, there is another specificity pocket (SP) near ABP, which is composed of residues W112, T114 and F123 from loop A and C299, A300, L301, L302, S303 and Y310 from loop C. W112 occupies the hinge area with privileged position between the anion binding pocket and allosteric binding pocket.

The structure characterization (from empirical data and molecular docking of AKR1B10 and AR in combination with specific inhibitors) has allowed to identify two key differences between AR and AKR1B10. The first one corresponds to a different conformation of the residue W112, and W112 adopts natural conformation through a hydrogen bond network, which includes residues Q114 and S304 located in loop C in AR, but

this network cannot be established in AKR1B10 (Fig. 3A and C). The reason why the conformation of W112 in Fig. 3B and C as the same is that the structure is that these conformations are obtained by the IFD method. Another difference is that the residues located in loop C, such as Q(S)303 and S(C)304. The residue W112 also forms $\pi-\pi$ stacking interaction in AKR1B10 and AR binding the inhibitors Zopolrestat, MK184 and MK204, but cannot be established in Fidarestat binding AKR1B10 and AR. It is worth mentioning that we can't get the complex structure of MK204 binding AR by Glide docking, but by IFD. The reason may be that the volume of MK204 is too large to accommodate the binding sites of AR, so we tried to obtain the stable conformation of MK204 binding to AR by using long distance MD.

3.2 Evaluation of inhibitors binding to AKR1B10 and AR from MD simulations

3.2.1 MD simulations. Accuracy and reliability of four inhibitors docking poses with AKR1B10 and AR were accessed by all atom explicit solvent MD simulations, and a total of 1 μ s simulation trajectories was collected. The RMSD of the eight complexes were observed by monitoring their values computed on the backbone atoms of protein and the heavy atoms of ligand in the simulation process. As shown in the Fig. S1,[†] after \sim 800 ns, both the heavy atoms of the inhibitor and the residues within 5 \AA of binding pocket have experienced relatively small conformational changes (RMSD $< 1 \text{\AA}$), which indicated that each complex reached an equilibrium state. However, the

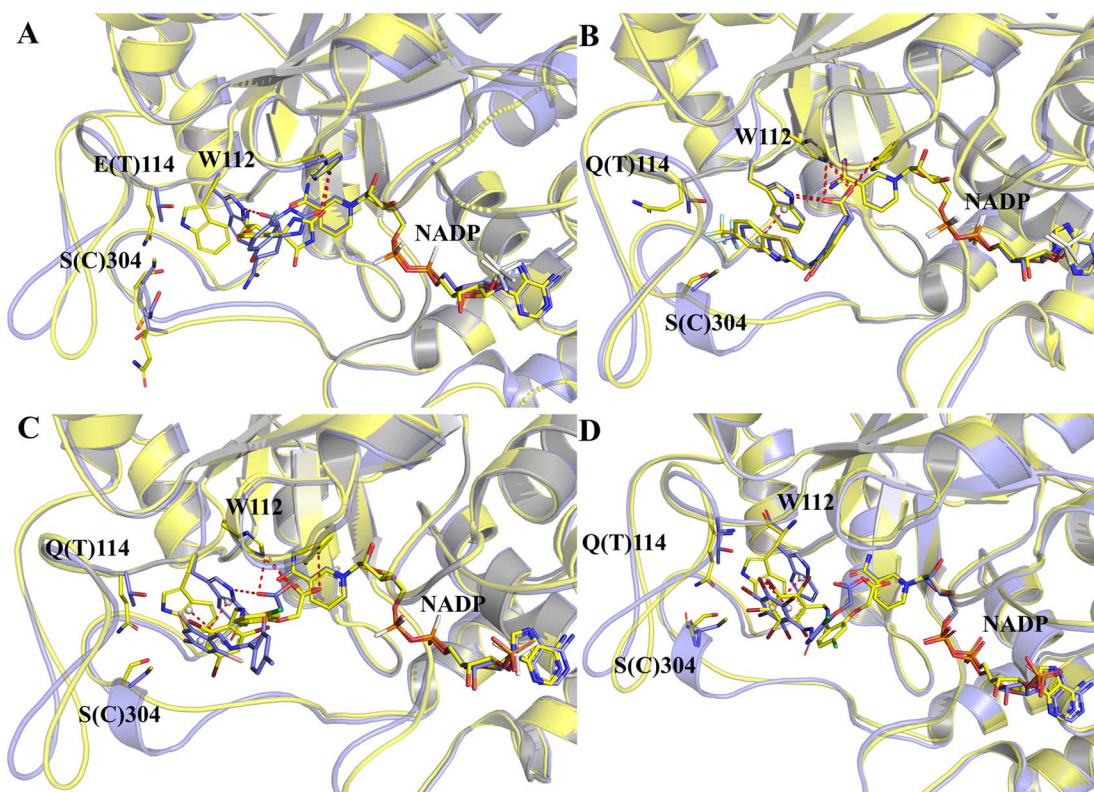


Fig. 3 The docking poses of four ligands Fidarestat (A), Zopolrestat (B), MK184 (C) and MK204 (D) with AKR1B10 and AR.



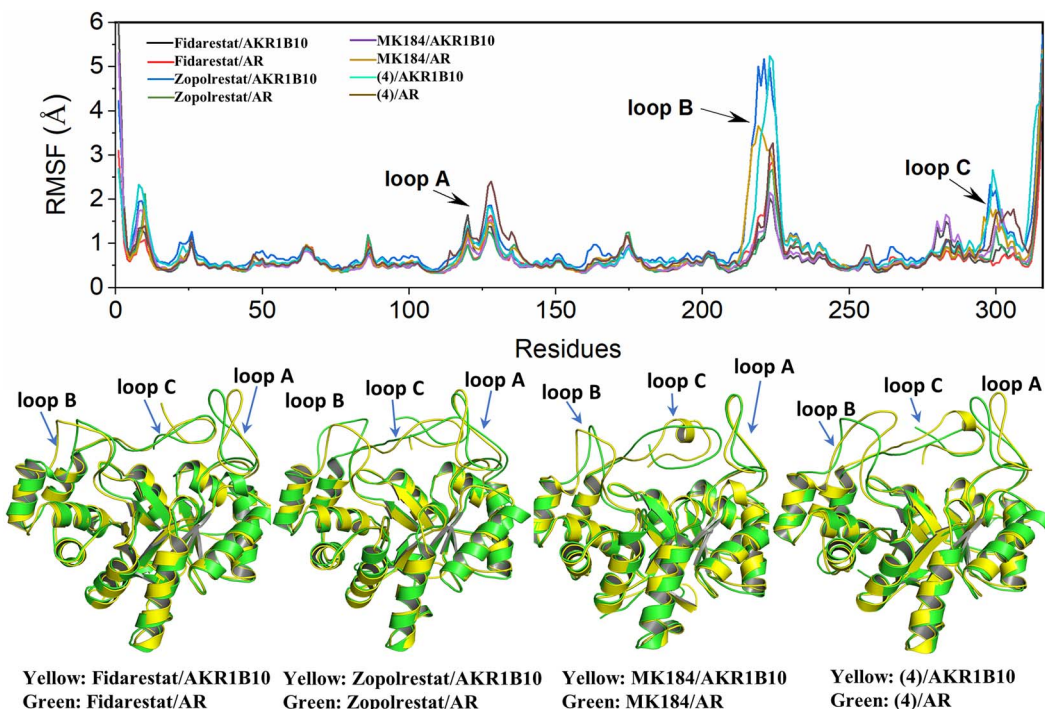


Fig. 4 Monitoring the fluctuations of RMSF of the protein of backbone in MD simulations.

backbone atoms of the protein have been fluctuating greatly, which is often related to the loop region in the protein structure. In addition, we also computed the RMSF values of the backbone eight complexes, and extracted the average structure of the complex from the last 200 ns. As shown in Fig. 4, the three-segment loop regions (loop A, loop B and loop C) show great fluctuations in all complexes. In order to observe the changes of the binding mode of inhibitor and protein during the whole MD process, we superimposed the average structure deriving from the last 100 ns in MD trajectory and the initial pose (Fig. S2†). For the compounds in com4, com6, com7 and com8, the largest conformation change is due to the deviation of carboxyl cation from the original binding site due to the change of carbon atom (marked in red in Fig. 1) conformation, which is also the reason for the great fluctuation of the heavy atoms of ligand and the residues within 5 Å of binding pocket in RMSD monitoring.

3.2.2 Profiles of inhibitors binding free energies in complex with AKR1B10 and AR. In order to explore the binding of studied inhibitors binding to AKR1B10 and AR, we calculated the binding free energy between receptors and ligands in eight complexes and its various components contributing to the binding free energy (ΔG_{bind}) by MM/PBSA method. The calculation results are summarized in Table 1. Obviously, in all cases, van der Waals interaction (ΔE_{vdw}) and electrostatic interaction (ΔE_{ele}) are the most important factors that promote the binding of receptors and ligands. The nonpolar solvation free energy (ΔG_{SA}) is favorable for the formation of receptor and ligand, while the polar solvation free energy (ΔG_{PB}) is not conducive to the formation of complexes. Entropy ($T\Delta S$) also opposes the binding of inhibitors to receptor. As shown in Table 1, there is no apparent difference in the calculated binding free energy between Fidarestat/AKR1B10 and Fidarestat/AR complexes, but there are

Table 1 Binding free energy predicted by MM/PBSA method

Contribution	Fidarestat/AKR1B10	Zopolrestat/AKR1B10	Zopolrestat/AR	MK184/AKR1B10	MK184/AR	MK204/AKR1B10	MK204/AR
ΔE_{ele}	-23.25 ± 0.17	-22.58 ± 0.15	-8.38 ± 0.24	-18.61 ± 0.23	-16.24 ± 0.17	-9.92 ± 0.11	-50.63 ± 0.18
ΔE_{vdw}	-28.80 ± 0.09	-27.57 ± 0.10	-44.65 ± 0.14	-47.05 ± 0.13	-48.35 ± 0.15	-46.62 ± 0.14	-76.95 ± 0.11
ΔG_{SA}	-3.97 ± 0.01	-3.58 ± 0.01	-5.19 ± 0.02	-5.08 ± 0.01	-5.50 ± 0.01	-4.71 ± 0.01	-5.31 ± 0.01
ΔG_{GB}	33.92 ± 0.12	31.28 ± 0.09	24.08 ± 0.22	30.01 ± 0.22	29.51 ± 0.14	22.8 ± 0.16	87.40 ± 0.16
$\Delta G_{\text{nonpolar}}^a$	-32.77 ± 0.09	-31.15 ± 0.14	-49.84 ± 0.14	-52.13 ± 0.13	-53.85 ± 0.15	-51.33 ± 0.14	-82.86 ± 0.11
$\Delta G_{\text{polar}}^b$	10.67 ± 0.21	8.70 ± 0.17	15.70 ± 0.37	11.40 ± 0.31	13.27 ± 0.22	12.88 ± 0.19	36.77 ± 0.24
ΔG_{Total}	-22.10 ± 0.11	-22.45 ± 0.11	-34.14 ± 0.15	-40.73 ± 0.11	-40.58 ± 0.14	-38.45 ± 0.12	-45.49 ± 0.11
$-T\Delta S$	17.73 ± 3.65	17.79 ± 4.67	24.14 ± 4.71	24.97 ± 2.55	20.14 ± 3.93	21.30 ± 6.46	19.23 ± 4.39
ΔG_{Bind}	-4.37 ± 3.66	-4.66 ± 4.68	-9.90 ± 4.72	-15.76 ± 2.56	-20.44 ± 3.94	-17.15 ± 6.47	-26.26 ± 4.40

^a $\Delta G_{\text{nonpolar}} = \Delta E_{\text{vdw}} + \Delta G_{\text{SA}}$. ^b $\Delta G_{\text{polar}} = \Delta E_{\text{ele}} + \Delta G_{\text{GB}}$.



apparent differences between Zopolrestat/AKR1B10 and Zopolrestat/AR complexes. The difference between them is mainly manifested in the electrostatic component, which leads to a great difference in the final binding free energy (ΔG_{bind} for Zopolrestat/AR is obviously lower than that for Zopolrestat/AKR1B10). This indicates that Fidarestat and Zopolrestat have no apparent selectivity to AKR1B10 and AR, which is consistent with the experimental data of inhibitory activity.

As compounds with apparent selective inhibitory effect on AKR1B10, MK184 and MK204 have apparent difference in binding AKR1B10 and AR. This difference is mainly reflected in the electrostatic component, and van der Waals' contribution to the binding free energy also accounts for the main part, while the entropy contribution has little change. The binding free energy (ΔG_{bind}) of MK184/AKR1B10 ($-20.44 \text{ kcal mol}^{-1}$) is lower than that of MK184/AR ($-17.15 \text{ kcal mol}^{-1}$), which also is agreement with the experiment data. MK204 is found to have the highest selectivity to AKR1B10 in experiment, and our calculated ΔG_{bind} of MK204/AKR1B10 and MK204/AR is $-26.26 \text{ kcal mol}^{-1}$ and $-19.67 \text{ kcal mol}^{-1}$, respectively. Electrostatic component (ΔE_{ele}) and van der Waals' contribution (ΔE_{vdw}) drive this difference ($-127.58 \text{ kcal mol}^{-1}$ for MK204/AKR1B10 and $-55.98 \text{ kcal mol}^{-1}$ for MK204/AR), and later we will analyze the reasons for the differences from energy decomposition and binding mode of all inhibitors with AKR1B10 and AR.

3.2.3 The importance of hydrogen bond interaction on the stability of inhibitors binding AKR1B10 and AR. Hydrogen bond play a critical role in stabilizing the receptor and ligand, so it

makes an important contribution to evaluating the affinity between receptor and ligand. We counted the hydrogen bond interactions between inhibitors and proteins in the equilibrium trajectories of eight complexes. The percentage occupancy of hydrogen bond determines the strength and stability of the hydrogen bond between the inhibitors and protein throughout the simulations (800–1000 ns) and listed in Table 2. It depicts that Fidarestat forms hydrogen bond with the residue Y49 in both AKR1B10 and AR with $\sim 70\%$ and $\sim 73\%$ occupancy in the simulations in agreement with the initial poses (Fig. 3). Similarly, the MK184/AKR1B10 complex exhibits $\sim 83\%$ occupancy of hydrogen bond between residue Y49 with MK184, and the MK204/AKR1B10 complex exhibits $\sim 82\%$ and $\sim 65\%$ occupancy of hydrogen bond between residues Y49 and H111 with MK204, suggesting the strong hydrogen bond formations between them while only $\sim 20\%$ of occupancy between residue H111 and MK184.

In Fidarestat/AKR1B10 and Fidarestat/AR complexes, several hydrogen bonds with low occupancy rate were also detected. For example, in Fidarestat/AKR1B10, residue N300 acted as hydrogen bond acceptor and donor, forming hydrogen bond with Fidarestat with $\sim 24\%$ and $\sim 28\%$ occupancy, respectively. Fidarestat forms hydrogen bond with residues W112, L301 and H111 with $\sim 64\%$, $\sim 37\%$ and $\sim 28\%$ occupancy respectively in Fidarestat/AR. Only $\sim 80\%$ of the hydrogen bond between Zopolrestat with AR were detected, while $\sim 44\%$ of the hydrogen bond of H111 were detected in MK184/AKR1B10 besides the hydrogen bond between Y49 and MK184. On the contrary, only $\sim 20\%$ of hydrogen bond between MK184 and H111 were found, which supported the

Table 2 Summary of hydrogen bond between the ligand and protein

Acceptor	DonorH	Donor	Frac ^a (%)	AvgDist ^b (Å)	AvgAng ^b
Fidarestat/AKR1B10					
N300(O)	Ligand(H10)	Ligand(N3)	0.23	2.89	155.47
Ligand(O2)	Y49(HH)	Y49(OH)	0.70	2.76	163.68
Ligand(O3)	Asn300(H)	N300(N)	0.28	2.91	164.13
Fidarestat/AR					
Ligand(O4)	Y49(HH)	W49(OH)	0.73	2.76	163.62
Ligand(O3)	W112(HE1)	W112(NE1)	0.64	2.85	157.02
Ligand(O2)	L301(H)	L301(N)	0.37	2.88	149.89
Ligand(O4)	H111(HE2)	H111(NE2)	0.28	2.88	146.62
Zopolrestat/AR					
Ligand(O1)	A300(H)	A300(N)	0.71	2.85	163.72
MK184/AKR1B10					
Ligand(O2)	Y49(HH)	Y49(OH)	0.83	2.71	164.29
Ligand(O4)	H111(HE2)	H111(NE2)	0.44	2.85	150.19
MK184/AR					
Ligand(O4)	H111(HE2)	H111(NE2)	0.20	2.86	159.36
MK204/AKR1B10					
Ligand(O3)	Y49(H)	Y49(OH)	0.82	2.65	168.56
Ligand(O4)	Y49(HH)	Y49(OH)	0.17	2.64	168.26
Ligand(O4)	H111(HE2)	H111(NE2)	0.66	2.80	152.90
Ligand(O3)	H111(HE2)	H111(NE2)	0.20	2.82	153.18

^a The frequency of the hydrogen bond in 20 000 conformations is counted. ^b Distance and angle of hydrogen bond.



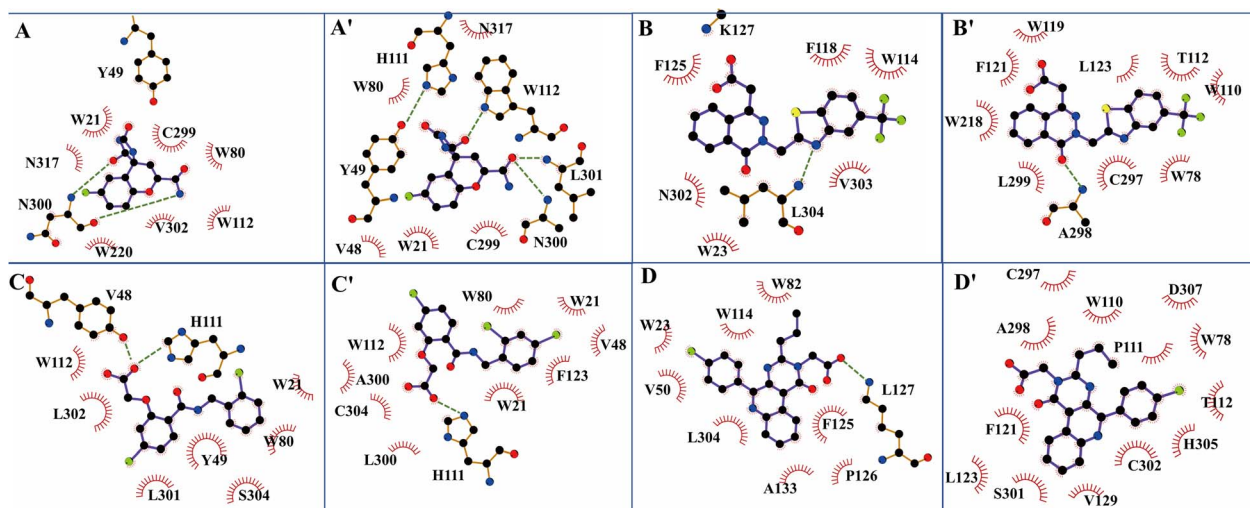


Fig. 5 Residues that form hydrophobic and hydrogen bond with ligands at the binding sites predicted by the LigPlus. Fidarestat binding AKR1B10 (A) or AR (A'), Zopolrestat binding AKR1B10 (B) or AR (B'), MK184 binding AKR1B10 (C) or AR (C') and MK204 binding AKR1B10 (D) or AR (D').

numerical difference of predicted binding free energy between Zopolrestat and MK184 with AKR1B10(AR). No hydrogen bond formation with high occupancy was observed in Zopolrestat/AKR1B10, MK184/AR and MK204/AR (Fig. 5).

3.3 Identification of interactions crucial for binding and inhibitory activities of AKR1B10 inhibitory

3.3.1 Comparison of bound modes of Fidarestat and Zopolrestat with AKR1B10 and AR. The energy contribution of each residue for the complexes was calculated based on equilibrated MD simulation trajectories. As shown in Fig. 6, residues

W21, V48, H111, W112, N161, C299 and L302 at the binding site of AKR1B10 and AR were identified as key residues (with difference of the absolute energy contribution of ≥ 0.5 kcal mol $^{-1}$) for Fidarestat binding AKR1B10 and AR. There is no obvious difference between the calculated binding free energies of the two molecular complexes. Due to the inversion of residue W112 conformation, the binding of Fidarestat to AKR1B10 is slightly different from that of AR, which makes these key residues show different effects on Fidarestat. For example, Fidarestat forms hydrogen bond with residues Y49 and N300 in AKR1B10, while it has hydrogen bond with the

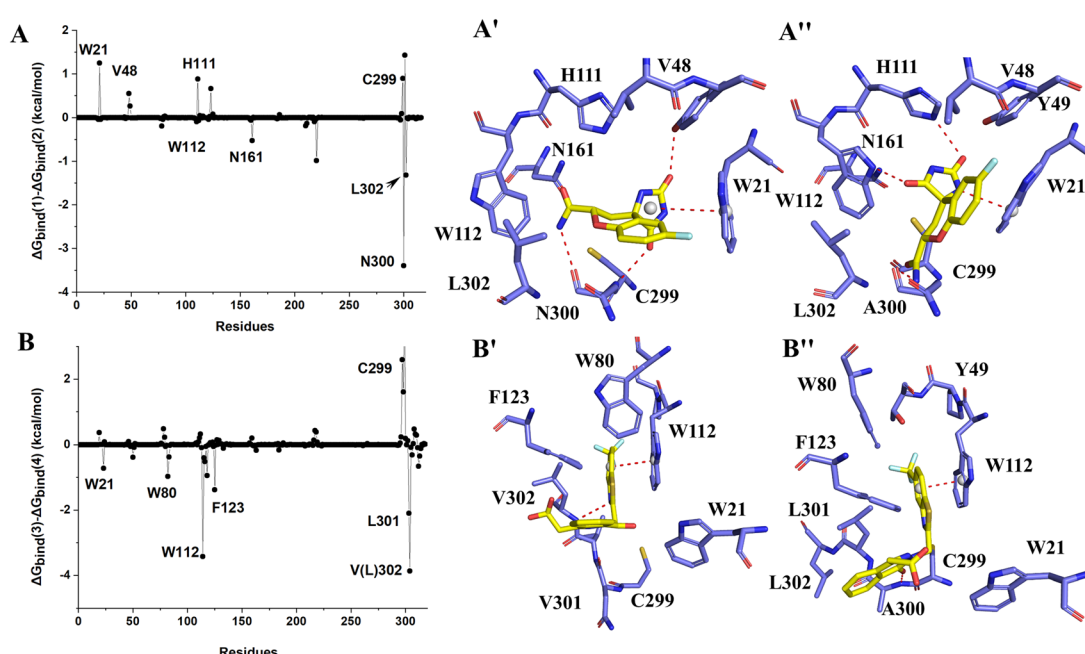


Fig. 6 Per-residue interaction decomposition of the binding free energies for (A) Fidarestat/AKR1B10(AR) and (B) Zopolrestat/AKR1B10(AR). Comparison of the binding modes of Fidarestat with AKR1B10 (A') and AR (A''), Zopolrestat(F) with AKR1B10 (B') and AR (B''), respectively. The purple sticks represent the important residues and the yellow sticks represent the ligands.

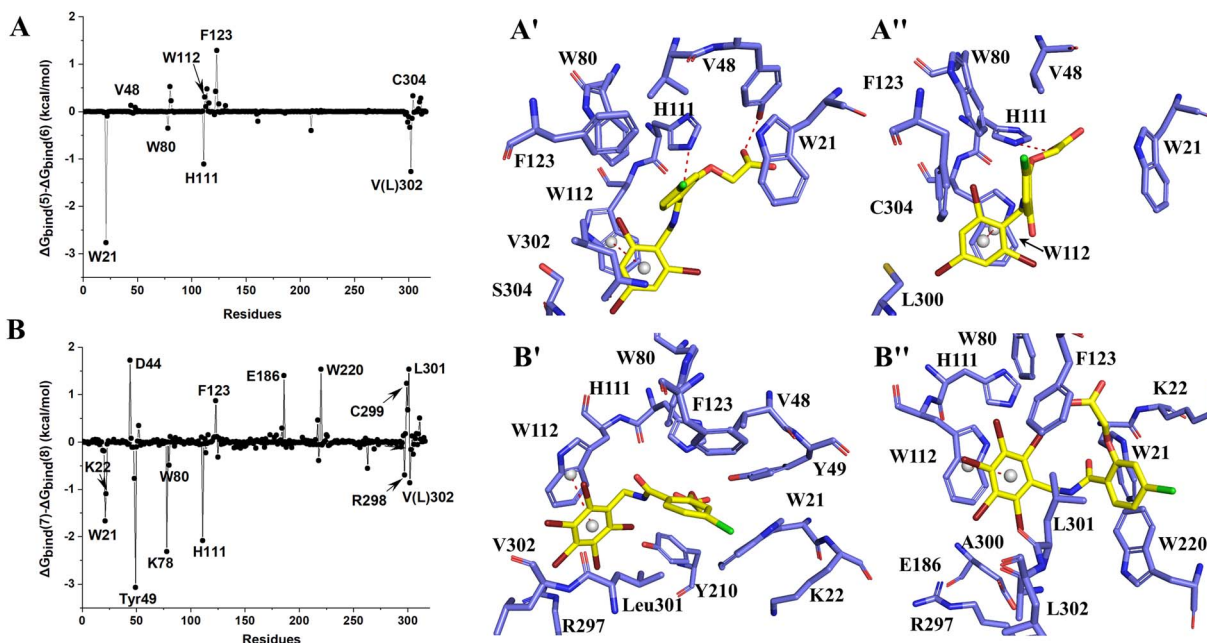


Fig. 7 Per-residue interaction decomposition of the binding free energies for (A) MK184/AKR1B10(AR) and (B) MK204/AKR1B10(AR). Comparison of the binding modes of MK184 with AKR1B10 (A') and AR (A''), MK204 with AKR1B10 (B') and AR (B''), respectively. The purple sticks represent the important residues and the yellow sticks represent the ligands.

residues Y49, W112, H111 and L301 in AR (Table 2). W21 forms π - π stacking interaction with Fidarestat in both AKR1B10 and AR. So, there is no apparent difference between the calculated ΔG_{bind} of the two complexes.

The binding free energies of Zopolrestat/AR estimated by MM/PBSA are relatively lower than that of Zopolrestat/AKR1B10, which is closely consistent with the experimental data. The Fig. 6 shows that almost all the residues W21, W80, W112, F123, V301 and V302 have stronger interactions with Zopolrestat than that with AR, are these residues are hydrophobic interaction. Unlike the binding mode of Fidarestat with AKR1B10(AR), Zopolrestat is far from residue W21, and forms π - π stacking interaction with W112 in both AKR1B10 and AR. The side chain conformation of W112 has always remained the same as the initial structure, while Zopolrestat's carboxylic acid group deviated from ABP, which made it form π - π stacking interaction with W218 and remained stable.

3.3.2 Comparison of binding modes of MK184 and MK204 with AKR1B10 and AR. As shown in Fig. 7, V48, W80, H111, W112, F123, L302 and C304 are the key residues in MK184 binding AKR1B10 and AR, and also from the binding modes of MK184 with AKR1B10 and AR we can see that the binding of MK184 with AKR1B10 has been very stable, and the conformation of MK184 has not changed obviously in the whole molecular dynamics simulation trajectory compared with the initial conformation. However, the polybrominated aryl portion of MK184 is too large to be suitable for ABP of AR, because the conformation changes obviously during the interaction with AR (Fig. 7B''). The aryl moiety of MK184 is having a tight fit with the loop A (F123 located in here), and MK184 can fit nicely into a novel AR binding site conformer, mainly through π - π

stacking interaction with the W112. Computational studies paired with the structures allowed us to surmise that ligand binding in this novel pocket requires a very hydrophobic aryl moiety. The loop A is usually driven by the hydrophobic part of the inhibitor. To realize this opening, the loop C shows a high degree of flexibility. Binding in this flexible region is unfavorable to improve the binding affinity of drugs to targets.

MK204 showed similar behavior to MK184 in binding with AKR1B10 and AR. The benzene ring of MK204 accumulated to the bottom of loop A in the process of binding with AR, and the carboxyl group was far away from the original ABP due to the conformation inversion of the benzene ring, while it was stable with the residue W220 on loop B in the cavity formed by loop A, B and C through the π - π stacking interaction. The difference of this binding mode can also be observed from the energy decomposition spectrum. Clearly, the residues that are more favorable for the binding of MK204 to AR include F123, W220, C299 and L301, while the residues that are more favorable for the binding of MK204 to AR, such as W21, K22, Y49, K78, W80, H111, R298 and V302. Both MK204 and MK184 deviate from the original binding sites when they bind to AR, which indicates that the existence of hydrophobic benzene ring is beneficial to improve the selectivity to AKR1B10.

4. Conclusions

It is a great challenge to develop highly selective inhibitor of AKR1B10 to treat cancer. Understanding of protein-inhibitor interactions is of importance for designing targeted selective inhibitors. In this work, the binding of inhibitors with AKR1B10 and AR were investigated by molecular docking, MD



simulations and binding free energy calculations. The slight change of protein conformation may contribute to the selectivity of inhibitors to AKR1B10 and AR. By analyzing the binding mode and calculating the binding free energy of representative inhibitors to AKR1B10 and AR, we concluded that highly selective inhibitors of AKR1B10 should have the following features:

(1) The binding at the anion binding pocket (ABP) is important to the inhibitory activity: the hydrogen bonding between Y49 and the inhibitor and the π - π stacking between W112 and the inhibitor play a key role in the stability of the inhibitor and AKR1B10(AR), which contributes to the high inhibitory activity of AKR inhibitors. For example, when MK184 and MK204 binding to AR, their carboxyl groups deviated from ABP, resulting in a significant decrease in their inhibitory activity against AR.

(2) The hydrophobic effect of bulky phenyl enhancing the selectivity to AKR1B10: Zopolrestat, MK184 and MK204 deviate from ABP when they are combined with AR, but remain stable in AKR1B10, which indicates that benzene ring can enhance the selectivity to AKR1B10.

(3) Maintaining the native conformation of W112: the side chain conformation of W112 is different in the crystal structure of the studied inhibitors–AKR1B10(AR), and W112 keeps stable through π - π stacking interaction with the ligand in the whole MD simulations. However, the carboxylic acid group of the ligand deviates from ABP seriously in the inhibitor–AR complex, indicating that although the inhibitor keeps the conformation of W112 stable during the interaction with AR, this conformation is not suitable for stabilizing the inhibitor AKR1B10 complex.

Conflicts of interest

The authors declare that there is no conflict of interest in this work.

Acknowledgements

This work was supported by the Natural Foundation of Shandong Province (Grant No. ZR2022MB134).

References

- 1 S. Endo, T. Matsunaga and T. Nishinaka, *Metabolites*, 2021, **11**, 332.
- 2 L. Qiu and C. Guo, *Curr. Drug Targets*, 2020, **21**, 599–609.
- 3 M. Hojnik, S. Frković Grazio, I. Verdenik and T. L. Rizner, *Cancers*, 2021, **13**, 3398.
- 4 M. M. Bacha, H. Nadeem, S. Zaib, S. Sarwar, A. Imran, S. U. Rahman, H. S. Ali, M. Arif and J. Iqbal, *BMC Chem.*, 2021, **15**, 28.
- 5 S. Jannapureddy, M. Sharma, G. Yepuri, A. M. Schmidt and R. Ramasamy, *Front. Endocrinol.*, 2021, **12**, 636267.
- 6 A. Kousaxidis, A. Petrou, V. Lavrentaki, M. Fesatidou, I. Nicolaou and A. Geronikaki, *Eur. J. Med. Chem.*, 2020, **207**, 112742.
- 7 L. Quattrini and C. La Motta, *Expert Opin. Ther. Pat.*, 2019, **29**, 199–213.
- 8 J. M. Seliger, S. S. Cicek, L. T. Witt, H. J. Martin, E. Maser and J. Hintzpeter, *Molecules*, 2018, **23**, 3041.
- 9 W. Xu, Y. Gao, J. Zhang, R. Zhang and Q. Chen, *Oncol. Lett.*, 2021, **22**, 683.
- 10 Y. T. Chung, K. A. Matkowskyj, H. Li, H. Bai, W. Zhang, M. S. Tsao, J. Liao and G. Y. Yang, *Mod. Pathol.*, 2012, **25**, 758–766.
- 11 J. Breton, M. C. Gage, A. W. Hay, J. N. Keen, C. P. Wild, C. Donnellan, J. B. Findlay and L. J. Hardie, *J. Proteome Res.*, 2008, **7**, 1953–1962.
- 12 C. P. Li, A. Goto, A. Watanabe, K. Murata, S. Ota, T. Niki, H. Aburatani and M. Fukayama, *Pathol. Res. Pract.*, 2008, **204**, 295–304.
- 13 Y. Shen, J. Ma, R. Yan, H. Ling, X. Li, W. Yang, J. Gao, C. Huang, Y. Bu, Y. Cao, Y. He, L. Wan, X. Zu, J. Liu, M. C. Huang, W. F. Stenson, D. F. Liao and D. Cao, *Clin. Cancer Res.*, 2015, **21**, 1466–1476.
- 14 D. X. Luo, M. C. Huang, J. Ma, Z. Gao, D. F. Liao and D. Cao, *Biochem. J.*, 2011, **438**, 71–80.
- 15 O. L. Zinovieva, E. N. Grineva, G. S. Krasnov, D. S. Karpov, A. O. Zheltukhin, A. V. Snezhkina, A. V. Kudryavtseva, T. D. Mashkova and N. A. Lisitsyn, *J. Cancer*, 2019, **10**, 4256–4263.
- 16 L. Huang, R. He, W. Luo, Y. S. Zhu, J. Li, T. Tan, X. Zhang, Z. Hu and D. Luo, *Recent Pat. Anti-Cancer Drug Discovery*, 2016, **11**, 184–196.
- 17 J. Liu, G. Wen and D. Cao, *Recent Pat. Anti-Cancer Drug Discovery*, 2009, **4**, 246–253.
- 18 T. M. Penning, *Chem.-Biol. Interact.*, 2015, **234**, 236–246.
- 19 I. R. Edwards and J. K. Aronson, *Lancet*, 2000, **356**, 1255–1259.
- 20 B. Chen, H. Choi, L. J. Hirsch, A. Katz, A. Legge, R. Buchsbaum and K. Detyniecki, *Epilepsy Behav.*, 2017, **76**, 24–31.
- 21 A. Saxena, R. Tammali, K. V. Ramana and S. K. Srivastava, *Curr. Cancer Drug Targets*, 2018, **18**, 905–911.
- 22 D. Badawy, H. M. El-Bassossy, A. Fahmy and A. Azhar, *Can. J. Physiol. Pharmacol.*, 2013, **91**, 101–107.
- 23 A. Cousido-Siah, F. X. Ruiz, J. Fanfrlík, J. Giménez-Dejoz, A. Mitschler, M. Kamlar, J. Veselý, H. Ajani, X. Parés, J. Farrés, P. Hobza and A. D. Podjarny, *ACS Chem. Biol.*, 2016, **11**, 2693–2705.
- 24 I. Crespo, J. Giménez-Dejoz, S. Porté, A. Cousido-Siah, A. Mitschler, A. Podjarny, H. Pratsinis, D. Kletsas, X. Parés, F. X. Ruiz, K. Metwally and J. Farrés, *Eur. J. Med. Chem.*, 2018, **152**, 160–174.
- 25 L. Zhang, H. Zhang, Y. Zhao, Z. Li, S. Chen, J. Zhai, Y. Chen, W. Xie, Z. Wang, Q. Li, X. Zheng and X. Hu, *FEBS Lett.*, 2013, **587**, 3681–3686.
- 26 E. B. Miller, R. B. Murphy, D. Sindhikara, K. W. Borrelli, M. J. Grisewood, F. Ranalli, S. L. Dixon, S. Jerome, N. A. Boyles, T. Day, P. Ghanakota, S. Mondal, S. B. Rafi, D. M. Troast, R. Abel and R. A. Friesner, *J. Chem. Theory Comput.*, 2021, **17**, 2630–2639.
- 27 C. A. Sottriffer, *Curr. Top. Med. Chem.*, 2011, **11**, 179–191.



28 H. Steuber, M. Zentgraf, C. Gerlach, C. A. Sotriffer, A. Heine and G. Klebe, *J. Mol. Biol.*, 2006, **363**, 174–187.

29 O. El-Kabbani, C. Darmanin, T. R. Schneider, I. Hazemann, F. Ruiz, M. Oka, A. Joachimiak, C. Schulze-Briese, T. Tomizaki, A. Mitschler and A. Podjarny, *Proteins*, 2004, **55**, 805–813.

30 P. Cieplak, W. D. Cornell, C. Bayly and P. A. Kollman, *J. Comput. Chem.*, 1995, **16**, 1357–1377.

31 C. I. Bayly, P. Cieplak, W. Cornell and P. A. Kollman, *J. Phys. Chem.*, 1993, **97**, 10269–10280.

32 T. Fox and P. A. Kollman, *J. Phys. Chem.*, 1998, **102**, 8070–8079.

33 C. Tian, K. Kasavajhala, K. A. A. Belfon, L. Raguette, H. Huang, A. N. Migues, J. Bickel, Y. Wang, J. Pincay, Q. Wu and C. Simmerling, *J. Chem. Theory Comput.*, 2020, **16**, 528–552.

34 W. L. Jorgensen, J. Chandrasekhar, J. D. Madura, R. W. Impey and M. L. Klein, *J. Chem. Phys.*, 1983, **79**, 926–935.

35 A. C. Simmonett and B. R. Brooks, *J. Chem. Phys.*, 2021, **154**, 054112.

36 J.-P. Ryckaert, G. Ciccotti and H. J. C. Berendsen, *J. Comput. Phys.*, 1977, **23**, 327–341.

37 P. A. Kollman, I. Massova, C. Reyes, B. Kuhn, S. H. Huo, L. Chong, M. Lee, T. Lee, Y. Duan, W. Wang, O. Donini, P. Cieplak, J. Srinivasan, D. A. Case and T. E. Cheatham, *Acc. Chem. Res.*, 2000, **33**, 889–897.

38 P. D. Lyne, M. L. Lamb and J. C. Saeh, *J. Med. Chem.*, 2006, **49**, 4805–4808.

39 W. Xue, T. Fu, S. Deng, F. Yang, J. Yang and F. Zhu, *ACS Chem. Neurosci.*, 2022, **13**, 340–351.

40 J. Yang, X. Lin, N. Xing, Z. Zhang, H. Zhang, H. Wu and W. Xue, *J. Chem. Inf. Model.*, 2021, **61**, 3917–3926.

41 W. Xue, P. Wang, B. Li, Y. Li, X. Xu, F. Yang, X. Yao, Y. Z. Chen, F. Xu and F. Zhu, *Phys. Chem. Chem. Phys.*, 2016, **18**, 3260–3271.

42 T. V. Lee, R. D. Johnson, V. L. Arcus and J. S. Lott, *Proteins: Struct., Funct., Bioinf.*, 2015, **83**, 2052–2066.

43 N. Li, R. I. Ainsworth, B. Ding, T. Hou and W. Wang, *J. Chem. Inf. Model.*, 2015, **55**, 1400–1412.

44 S. Genheden and U. Ryde, *Expert Opin. Drug Discovery*, 2015, **10**, 449–461.

45 D. Pan, W. Xue, W. Zhang, H. Liu and X. Yao, *Biochim. Biophys. Acta, Gen. Subj.*, 2012, **1820**, 1526–1534.

46 D. Pan, Y. Niu, W. Xue, Q. Bai, H. Liu and X. Yao, *Chemom. Intell. Lab. Syst.*, 2016, **154**, 185–193.

47 A. Onufriev, D. Bashford and D. A. Case, *Proteins: Struct., Funct., Bioinf.*, 2004, **55**, 383–394.

48 M. Levitt, C. Sander and P. S. Stern, *J. Mol. Biol.*, 1985, **181**, 423–447.

